British Journal of Pharmacology

British Journal of Pharmacology (2017) **174** 2623–2635 2623

RESEARCH PAPER

Combination therapy with telmisartan and parecoxib induces regression of endometriotic lesions

Correspondence Matthias W. Laschke, Institute for Clinical & Experimental Surgery, Saarland University, D-66421 Homburg/Saar, Germany. E-mail: matthias.laschke@uks.eu

Received 3 January 2017; **Revised** 24 April 2017; **Accepted** 18 May 2017

Anca Nenicu, Yuan Gu, Christina Körbel, Michael D Menger and Matthias W Laschke

Institute for Clinical & Experimental Surgery, Saarland University, Homburg/Saar, Germany

BACKGROUND AND PURPOSE

Telmisartan suppresses the development of endometriotic lesions. However, the drug also up-regulates the expression of COX-2, which has been suggested to promote the progression of endometriosis. Accordingly, in the present study we analysed whether a combination therapy with telmisartan and a COX-2 inhibitor may be more effective in the treatment of endometriotic lesions than the application of telmisartan alone.

EXPERIMENTAL APPROACH

Endometriotic lesions were induced in the peritoneal cavity of C57BL/6 mice, which were treated daily with an i.p. injection of telmisartan (10 mg·kg^{-1}), parecoxib (5 mg·kg^{-1}), a combination of telmisartan and parecoxib or vehicle. Therapeutic effects on lesion survival, growth, vascularization, innervation and protein expression were studied over 4 weeks by high-resolution ultrasound imaging as well as immunohistochemical and Western blot analyses.

KEY RESULTS

Telmisartan-treated lesions exhibited a significantly reduced lesion volume when compared with vehicle-treated controls and parecoxib-treated lesions. This inhibitory effect of telmisartan was even more pronounced when it was used in combination with parecoxib. The combination therapy resulted in a reduced microvessel density as well as lower numbers of proliferating Ki67-positive cells and higher numbers of apoptotic cleaved caspase-3-positive stromal cells within the lesions. This was associated with a lower expression of COX-2, MMP-9 and p-Akt/Akt when compared with controls. The application of the two drugs further inhibited the ingrowth of nerve fibres into the lesions.

CONCLUSIONS AND IMPLICATIONS

Combination therapy with telmisartan and a COX-2 inhibitor represents a novel, effective pharmacological strategy for the treatment of endometriosis.

Abbreviations

AT_1, receptor angiotensin 1 receptor; eNOS, endothelial NOS

DOI:10.1111/bph.13874

Introduction

Endometriosis is a frequent gynaecological disease of women in reproductive age, which is characterized by the presence of endometrial-like tissue outside the uterine cavity (Giudice, 2010). The complex pathogenesis of the disease involves retrograde menstruation of oestrogen-sensitive endometrial cells and fragments into the abdominal cavity, where they implant on peritoneal surfaces and develop into endometriotic lesions (Burney and Giudice, 2012). This dynamic process is associated with inflammation (Jiang *et al.,* 2016), angiogenesis and vasculogenesis (Laschke *et al.,* 2011; Laschke and Menger, 2012), nerve fibre growth (Miller and Fraser, 2015), the formation of adhesions and scarring (Somigliana *et al.,* 2012). Consequently, patients often suffer from recurrent pain and infertility, which markedly affect their quality of life (Simoens *et al.,* 2012). Hence, there is an urgent need to identify novel approaches for an effective endometriosis therapy.

In a previous study, we demonstrated that combined blockade of **AT_1 receptors** and activation of **PPAR-γ** by the widely applied anti-hypertensive drug **telmisartan** suppresses the development of endometriosis in different rodent models of the disease (Nenicu *et al.,* 2014). Indeed, we found that daily treatment of mice with clinically well-tolerated doses of the compound inhibits the vascularization, immune cell infiltration and growth of murine endometriotic lesions, which were surgically induced by endometrial tissue transplantation. Of interest, gene expression profile analyses of these lesions further revealed a strong up-regulation of *Ptgs2* coding for PG-endoperoxide synthase 2, that is, **COX-2**, under telmisartan treatment (Nenicu *et al.,* 2014). This is a surprising finding considering the fact that COX-2 has been suggested to promote the development and progression of endometriosis (Buchweitz *et al.,* 2006; Banu *et al.,* 2008; Wu *et al.,* 2010). In addition, several studies have reported that selective COX-2 inhibitors have beneficial therapeutic effects on endometriotic lesion formation and endometriosis-associated pain (Cobellis *et al.,* 2004; Ozawa *et al.,* 2006; Laschke *et al.,* 2007; Machado *et al.,* 2010; Olivares *et al.,* 2013; Kilico *et al.,* 2014). Accordingly, in the present study we speculated that a combination therapy with telmisartan and a COX-2 inhibitor may be even more effective in the treatment of endometriosis than treatment with telmisartan alone.

To test our hypothesis, we surgically induced endometriotic lesions in the peritoneal cavity of mice, which were daily treated with vehicle, telmisartan, the selective COX-2 inhibitor **parecoxib** or a combination of the two drugs. Cyst formation and growth of the newly developing lesions were analysed by means of repetitive, high-resolution ultrasound imaging throughout an observation period of 4 weeks. Moreover, we assessed the vascularization, proliferation, viability, nerve fibre infiltration and protein expression of the lesions by means of immunohistochemistry and Western blot analyses.

Methods

Animals

The animal experiments of this study were approved by the governmental animal care committee of the Saarland, Germany (permit numbers: 53/11 and 25/12). They were conducted in accordance with the German legislation on protection of animals and the NIH Guidelines for the Care and Use of Laboratory Animals (NIH Publication #85-23 Rev. 1985). Also, animal studies are reported in compliance with the ARRIVE guidelines (Kilkenny *et al.*, 2010; McGrath and Lilley, 2015).

We used female C57BL/6 mice (Institute for Clinical & Experimental Surgery, Homburg/Saar, Germany) aged 3–4 months, with a body weight of 22–25 g. This animal strain has previously been used for the preclinical evaluation of telmisartan's effects on surgically-induced endometriotic lesions (Nenicu *et al.,* 2014). The animals were bred and housed in open cages (n = 4–5 per cage) on Lignocel® premium hygienic animal bedding (J. Rettenmaier & Söhne, Rosenberg, Germany) in the conventional animal husbandry of the Institute for Clinical & Experimental Surgery. They had free access to tap water and standard pellet food (Altromin, Lage, Germany). Before the surgical induction of endometriosis, oestrous cycling of individual mice was assessed by cytological analysis of vaginal lavage samples. For this purpose, 20 μL of physiological saline solution were pipetted into the vagina and transferred onto a glass slide for evaluation under a microscope (CH-2; Olympus, Hamburg, Germany). Only mice in the stage of oestrus were used as donor and recipient animals for the experiments to exclude confounding by different steroid hormone levels.

Endometriosis model

Peritoneal endometriotic lesions were induced by suturing uterine tissue samples to the abdominal wall, as described previously (Körbel *et al.,* 2010; Rudzitis-Auth *et al.,* 2012). This is a common model for the preclinical evaluation of drug effects on endometriotic lesions of standardized size and tissue composition (Becker *et al.,* 2006; Grümmer, 2006; Rudzitis-Auth *et al.,* 2013). For this purpose, 12 donor mice were anaesthetized by i.p. injection of ketamine (75 $mg \cdot kg^{-1}$ body weight; Ursotamin®; Serumwerk Bernburg, Bernburg, Germany) and xylazine (15 $mg \cdot kg^{-1}$ body weight; Rompun®; Bayer, Leverkusen, Germany). After laparotomy, the two uterine horns were harvested and transferred to a Petri dish containing DMEM (10% fetal calf serum, 1 $U \cdot mL^{-1}$ penicillin, 0.1 $mg \cdot mL^{-1}$ streptomycin; PAA, Cölbe, Germany). The horns were opened longitudinally, and 2 mm uterine tissue samples were removed by means of a dermal biopsy punch (Stiefel Laboratorium GmbH, Offenbach am Main, Germany). Two tissue samples were then sutured with 6-0 Prolene (Ethicon Products, Norderstedt, Germany) on each site of the abdominal wall of anaesthetized recipient mice through a midline incision (Figure 1A–D). Finally, the abdomen was closed with running 6–0 Prolene muscle and skin sutures. Subsequently, the animals were randomly assigned to the different treatment groups. The animals were treated daily with an i.p. injection of 10 $mg \cdot kg^{-1}$ telmisartan (n = 10), 5 $mg \cdot kg^{-1}$ parecoxib (n = 10) or telmisartan (10 $mg \cdot kg^{-1}$) in combination with parecoxib (5 $mg \cdot kg^{-1}$) (n = 10). Ten vehicle-treated animals (30 μL 5% DMSO i.p.) served as controls. The daily i.p. injections were well tolerated by the animals.

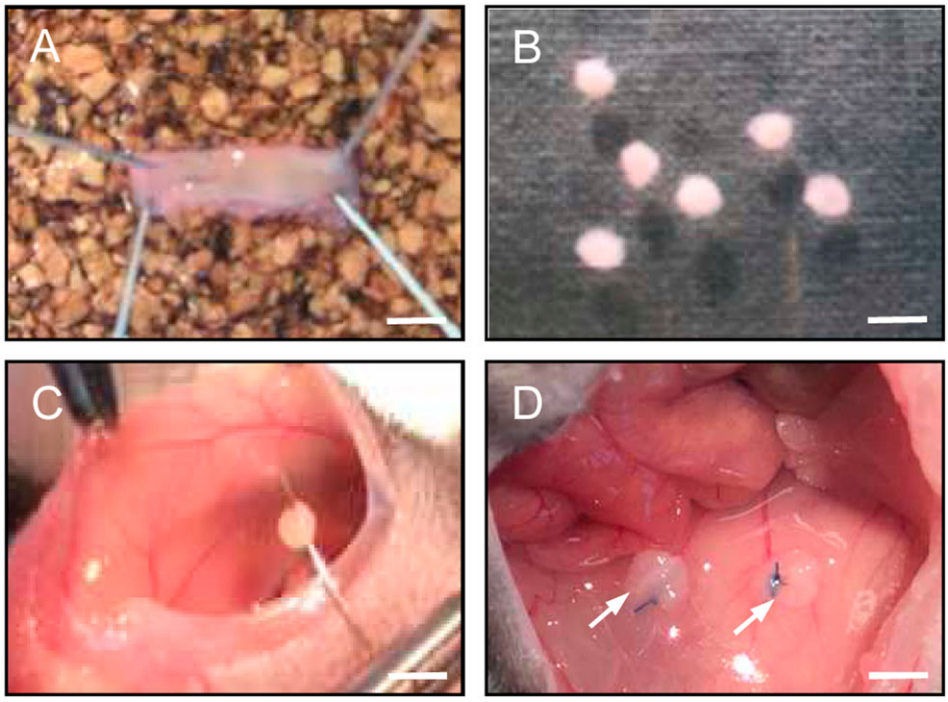

Figure 1

Surgical induction of murine endometriotic lesions in the peritoneal cavity. Uterine tissue samples (B) were isolated from the longitudinally opened uterine horn (A) of a donor mouse by means of a 2 mm dermal biopsy punch and sutured to the abdominal wall of a syngeneic recipient mouse (C). Typical appearance of the tissue samples directly after fixation (D, arrows). Scale bars: A = 5 mm; B = 2.5 mm; C = 3.3 mm; D = 2 mm.

High-resolution ultrasound imaging

The development of endometriotic lesions was analysed with a Vevo 770™ high-resolution ultrasound imaging system with a 704 Scanhead (40 MHz centre frequency) (VisualSonics, Toronto, ON, Canada) directly after surgical induction as well as on days 7, 14, 21 and 28 (Laschke *et al.*, 2010). The ultrasound images were analysed by means of a three-dimensional reconstruction and analysis software (Vevo 770 version 2.3.0; VisualSonics). The quantitative analysis included the measurements of the overall volume of endometriotic lesions as well as the volume of their cysts and stromal tissue (in mm^3) by manual image segmentation. For this purpose, boundaries of endometriotic lesions and their anechoic cysts were manually outlined in parallel slices, separated by a step size of 200 μm in the three-dimensional ultrasound images. Based on the outlined areas, volumes were subsequently computed by the VisualSonics software. In addition, we calculated the growth of lesions and stromal tissue (as % of the initial lesion and stromal tissue size) to identify the regression of lesions in individual groups, and we assessed the fraction of cyst-containing lesions (as % of all analysed lesions) (Rudzitis-Auth *et al.*, 2013). After the last ultrasound imaging on day 28, the animals were killed with 200 $mg \cdot kg^{-1}$ pentobarbital i.p. (Narcoren; Merial GmbH, Halbermoos, Germany) and the lesions were excised for further immunohistochemical and protein expression analyses.

Immunohistochemistry

Formalin-fixed specimens of the endometriotic lesions were embedded in paraffin and 3 μm-thick sections were cut. For immunofluorescent microscopic detection of PPAR-γ expression, sections were stained with a polyclonal rabbit anti-mouse antibody against PPAR-γ (1:100; ab19481; Abcam, Cambridge, UK). A goat anti-rabbit IgG Alexa Fluor 488 antibody (1:300; A11008; Invitrogen, Life Technologies GmbH, Darmstadt, Germany) served as the secondary antibody. Sections solely incubated with the secondary antibody were used as negative controls. Cell nuclei were stained with Hoechst 33342 (1:500; Sigma-Aldrich, Taufkirchen, Germany).

For immunofluorescent microscopic detection of microvessels, the sections were stained with a monoclonal rat anti-mouse antibody against the endothelial cell marker CD31 (1:100; Dianova, Hamburg, Germany) followed by a goat anti-rat IgG cyanine 3 antibody (1:50; Dianova). Cell nuclei were stained with Hoechst 33342 (1:500; Sigma-Aldrich).

Additional sections were stained with a polyclonal rabbit antibody against the proliferation marker Ki67 (1:2000; Abcam), followed by a biotinylated goat anti-rabbit IgG antibody (ready-to-use; Abcam) and streptavidin-peroxidase conjugate (1:50; Sigma-Aldrich) and finalized by a 3-amino-9-ethylcarbazol substrate system (ready to use; Abcam). The sections were conterstained with Mayers hemalaun solution (HX948000; Merck, Darmstadt, Germany). Moreover, sections were stained with a polyclonal rabbit antibody against the apoptosis marker cleaved **caspase (casp)-3** (1:100; New England Biolabs, Frankfurt, Germany), followed by a biotinylated goat anti-rabbit IgG antibody (ready-to-use; Abcam) and

finished by streptavidin Alexa 555 (1:50; Life Technologies, Eugene, OR, USA).

To identify nerve fibres within the endometriotic lesions, sections were incubated with a polyclonal rabbit anti-PGP9.5 (1:100; Abcam) and a monoclonal rat anti-mouse antibody against CD31 (1:100; Dianova), followed by a secondary goat anti-rabbit Alexa 488 antibody (1:100; Life Technologies) and a goat anti-rat IgG cyanine 3 (1:50; Dianova) antibody. For each group, sections from 10 animals were analysed with a BX-60 microscope (Olympus) and a BZ-8000 microscopic system (Keyence, Osaka, Japan). Quantitative analyses included the measurement of the microvessel and nerve fibre density (mm^{-2}) as well as the fraction of Ki67-positive proliferating and cleaved caspase-3-positive apoptotic stromal and glandular cells (%). For the calculation of the microvessel and nerve fibre density, the overall number of CD31-positive microvessels and PGP9.5-positive nerve fibres on a lesion section was divided by the stromal lesion area. The fraction of proliferating and apoptotic cells (given as % of all analysed cells) was calculated by dividing the number of Ki67- and cleaved caspase-3-positive stromal or glandular cells on a lesion section by the overall number of stromal or glandular cells on this section multiplied by 100.

Western blot analysis

For Western blot analyses, endometriotic lesions were lysed with RIPA buffer (Thermo Scientific, Bremen, Germany) containing 0.5 mM PMSF and Protease Inhibitor Cocktail (1:75 vv^{-1}; Sigma-Aldrich) on ice for 1 min with mechanical homogenization (Ultra-Thurax). The lysate was then collected and centrifuged for 20 min at 13000× *g* (4°C). The supernatant was saved as whole protein fraction. Protein concentrations were determined using the Pierce BCA Protein Assay Kit (Thermo Scientific) with BSA as standard. Then, 10 μg protein per lane were separated on 8% SDS-PAGEs and transferred to a PVDF membrane (BioRad, Munich, Germany). After blockade of non-specific binding sites, membranes were incubated overnight at 4°C with a polyclonal rabbit anti-COX-2 antibody (1:500; Abcam), a polyclonal rabbit anti-cleaved caspase-3 antibody (1:100; Cell Signaling Technology, Munich, Germany), a monoclonal mouse antibody to vimentin (1:100, Abcam), a polyclonal mouse anti-MMP-9 antibody (1:100, R&D Systems, Wiesbaden-Nordenstadt, Germany), a monoclonal rabbit anti-mouse **Akt** antibody (1:500; Cell Signaling Technology), a polyclonal rabbit anti-phosphorylated (p)-Akt1/2/3 antibody (Ser^{473}; 1:100; Santa Cruz Biotechnology, Heidelberg, Germany), a polyclonal rabbit anti-**ERK1/2** antibody (1:500; Cell Signaling Technology), a monoclonal mouse anti-human p-44/42 MAPK (p-ERK-1/2) antibody (1:500; Cell Signaling Technology), a monoclonal rabbit anti-mouse **endothelial NOS (eNOS)** antibody (1:100; BD Biosciences, Heidelberg, Germany), a monoclonal rabbit anti-mouse p-eNOS antibody (1:500; Cell Signaling Technology) and a polyclonal rabbit anti-cyclin D1 antibody (1:100; Santa Cruz Biotechnology), followed by the corresponding HRP-conjugated secondary antibodies (1:3000; GE Healthcare, Freiburg, Germany). Protein expression was visualized with ECL Western blotting substrate (GE Healthcare), and images were acquired using a Chemocam device (Intas, Göttingen, Germany). The intensity of immunoreactivity was assessed using Image J software (US National Institutes of Health) and normalized to tubulin signals as an internal standard. The Western blot analyses included six animals per group (two lesions per animal were pooled for one sample).

Data and statistical analyses

The data and statistical analysis comply with the recommendations on experimental design and analysis in pharmacology (Curtis *et al.*, 2015). To guarantee a blinded data analysis, all images and samples were recorded by a second person. Data were first analysed for normal distribution by means of the Shapiro–Wilk test and for equal variance. In the case of parametric data, differences between the experimental groups were assessed by one-way ANOVA followed by the Student–Newman–Keuls test, including the correction of the α-error according to Bonferroni probabilities. For non-parametric data, differences were assessed by ANOVA on ranks followed by Dunn's test (SigmaPlot version 13.0; Jandel Corporation, San Rafael, CA, USA). The *post hoc* tests were run only when F achieved $P < 0.05$. There was no significant variance in homogeneity. For a better clarity of data presentation, parametric and non-parametric data are given as mean ± SEM of at least six determinations per experimental group. Statistical significance was accepted for a value of $P < 0.05$.

Nomenclature of targets and ligands

Key protein targets and ligands in this article are hyperlinked to corresponding entries in http://www.guidetopharmacology.org, the common portal for data from the IUPHAR/BPS Guide to PHARMACOLOGY (Southan *et al.*, 2016), and are permanently archived in the Concise Guide to PHARMACOLOGY 2015/16 (Alexander *et al.*, 2015a,b,c).

Results

High-resolution ultrasound analysis of endometriotic lesions

High-resolution ultrasound imaging allowed the repetitive, non-invasive visualization of newly developing endometriotic lesions (Figure 2). After fixation to the abdominal wall, uterine tissue samples of all four experimental groups exhibited an initial size of ~1 mm^3 (Figure 2E). Throughout the observation period of 28 days, the sizes of control and parecoxib-treated lesions progressively increased to a final volume of 3.5–4 mm^3 (Figure 2A, B, E, F). This was caused by the proliferation of the stromal tissue (Figure 2G, H).

Telmisartan treatment suppressed the development of endometriotic lesions. They exhibited a significantly reduced lesion volume and stromal tissue volume on day 28 when compared with control and parecoxib-treated lesions (Figure 2C, E, G). Accordingly, calculated lesion and stromal tissue growth rates were also significantly reduced in telmisartan-treated animals (Figure 2F, H). Importantly, this inhibitory effect of telmisartan was more pronounced in combination with parecoxib treatment (Figure 2D–H). In contrast to the other treatments, the combination therapy

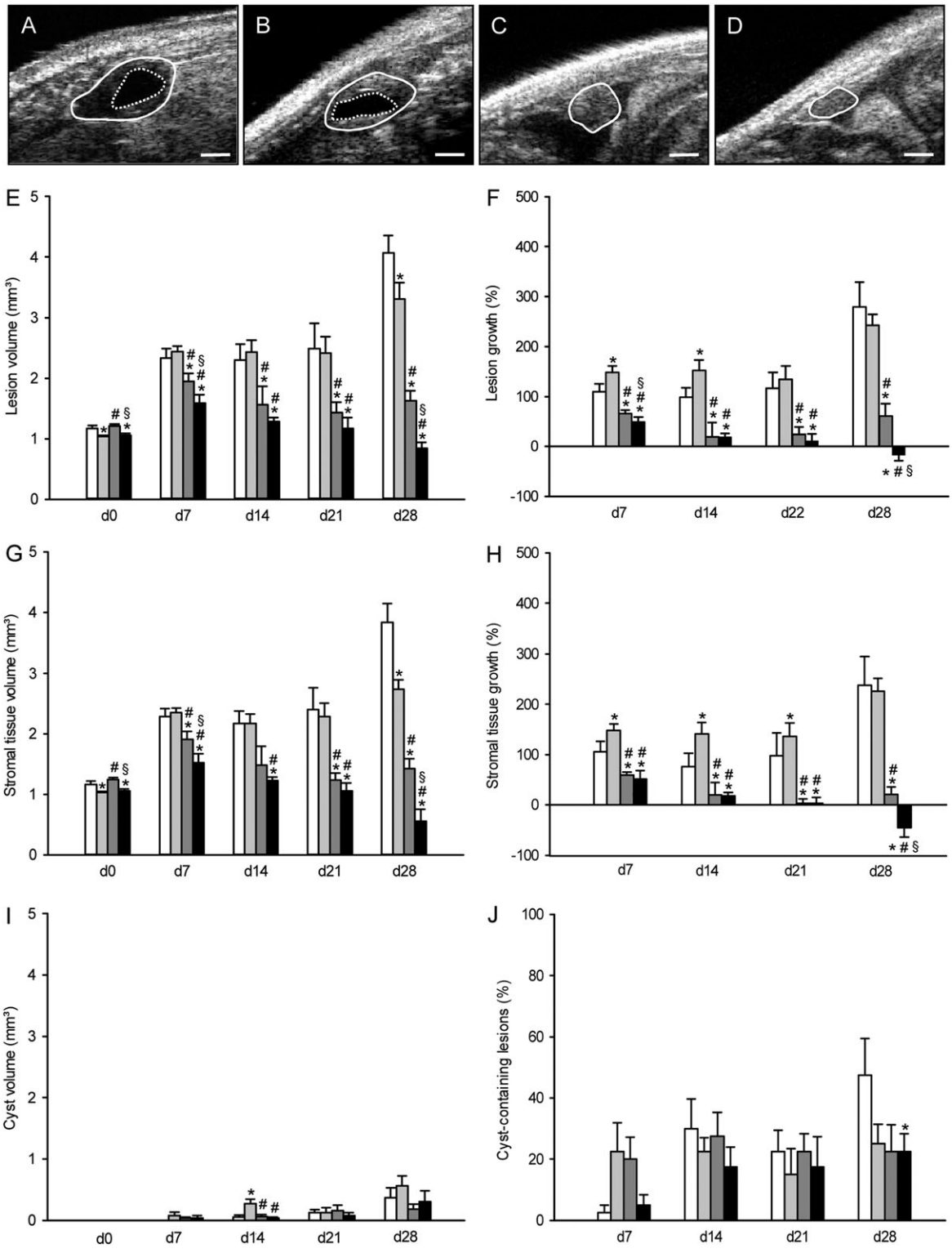

Figure 2

Ultrasound analysis of endometriotic lesions. High-resolution ultrasound imaging of endometriotic lesions (borders marked by closed line, cysts marked by broken line) 28 days after transplantation of uterine tissue samples into the peritoneal cavity of a vehicle-treated control (A), a parecoxib- (B), a telmisartan- (C) and a parecoxib/telmisartan- (D) treated C57BL/6 mouse. Scale bars: 500 μm. Lesion volume (E, mm^3), lesion growth (F, %), stromal tissue volume (G, mm^3), stromal tissue growth (H, %), cyst volume (I, mm^3) and fraction of cyst-containing lesions (J, %) of C57BL/6 mice, which were treated with vehicle (control, white bars), parecoxib (light grey bars), telmisartan (dark grey bars) or parecoxib/telmisartan (black bars) throughout an observation period of 28 days. Means ± SEM ($n = 10$ for each experimental group). *$P < 0.05$ versus control; $^{\#}P < 0.05$ versus parecoxib; $^{\S}P < 0.05$ versus telmisartan.

with telmisartan and parecoxib even resulted in negative lesion and stromal tissue growth rates on day 28 (Figure 2F, H), indicating a regression of the transplanted uterine tissue samples throughout the time course of the experiment.

Additional analyses of cyst formation in the developing endometriotic lesions revealed no marked differences between the experimental groups (Figure 2I, J). However, the rate of cyst-containing lesions in vehicle-treated animals on

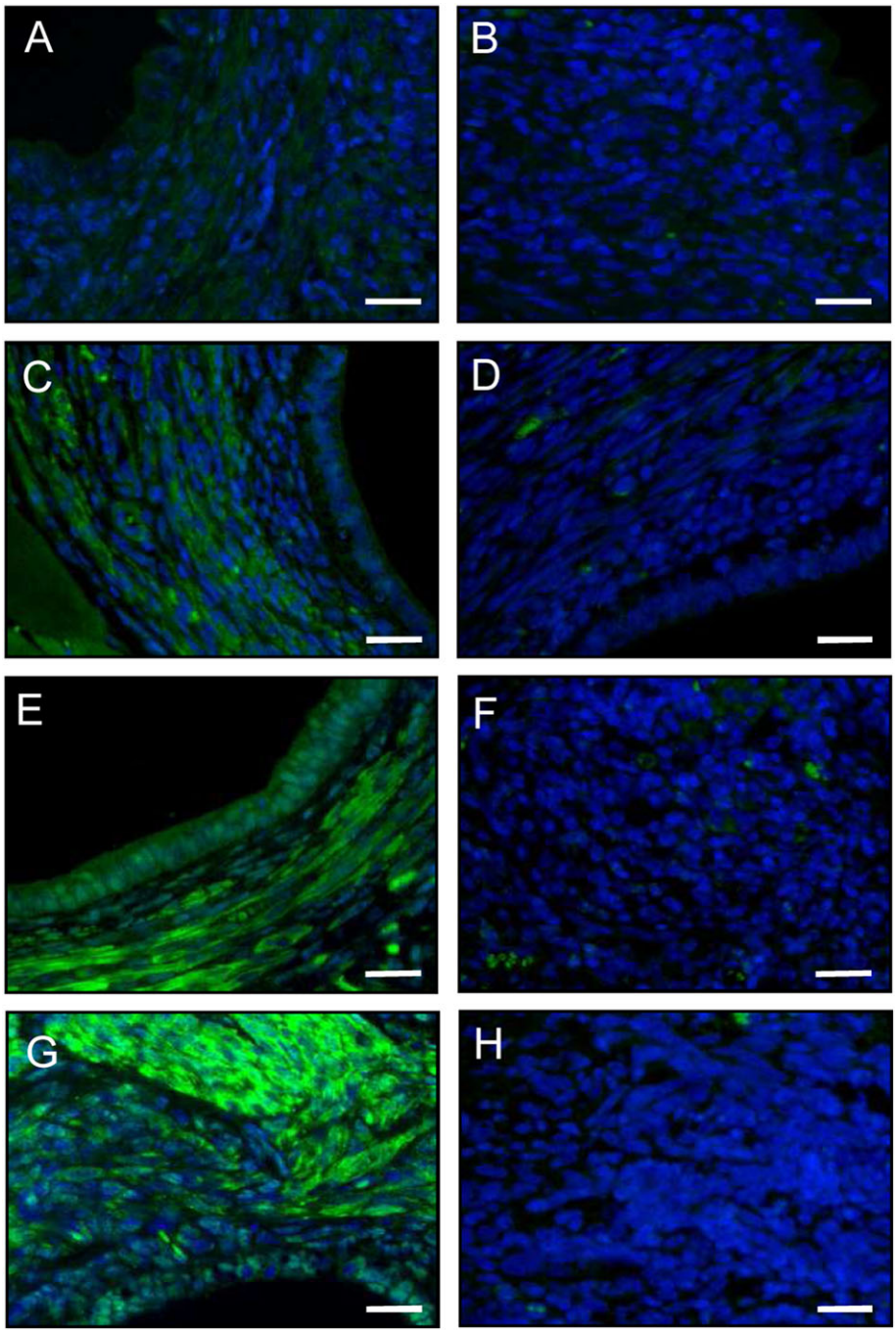

Figure 3

Immunofluorescence analysis of PPAR-γ expression within endometriotic lesions. Immunofluorescent detection of PPAR-γ within endometriotic lesions on day 28 after surgical induction by fixation of uterine tissue samples to the abdominal wall of a vehicle-treated control (A, B) as well as a parecoxib- (C, D), a telmisartan- (E, F) and a parecoxib/telmisartan- (G, H) treated C57BL/6 mouse. Sections were stained with Hoechst 33342 to identify cell nuclei (blue) and an antibody against PPAR-γ (green). Sections solely incubated with the secondary antibody served as negative controls (B, D, F, H; green signals = autofluorescence of erythrocytes). Scale bars: 20 μm.

day 28 was higher when compared with that in telmisartan/parecoxib-treated animals.

Immunohistochemical analysis of endometriotic lesions

At the end of the *in vivo* experiments, that is, on day 28, the newly developing endometriotic lesions were further processed for additional immunohistochemical analyses. These analyses revealed that treatment of the lesions with parecoxib slightly increased the stromal expression of PPAR-γ when compared with vehicle-treated controls (Figure 3A–D). This effect was even more pronounced in telmisartan-treated lesions (Figure 3E, F). Of interest, the combination therapy with telmisartan and parecoxib resulted in the strongest stromal and glandular expression

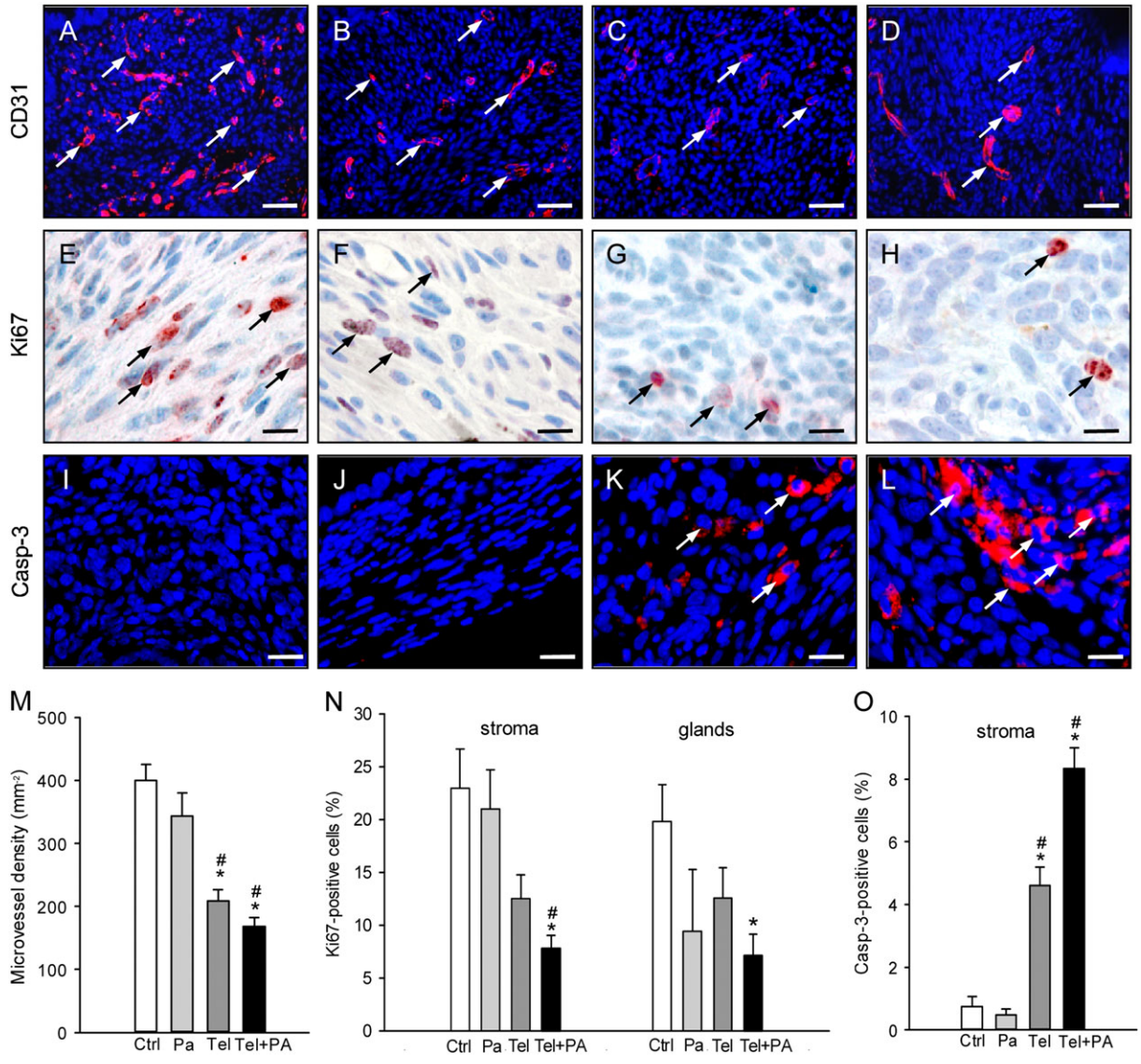

Figure 4

Immunohistochemical analysis of vascularization, cell proliferation and apoptotic cell death within endometriotic lesions. Immunofluorescent detection of microvessels (arrows) within endometriotic lesions on day 28 after surgical induction by fixation of uterine tissue samples to the abdominal wall of a vehicle-treated control (A) as well as a parecoxib- (B), a telmisartan (C) and a parecoxib/telmisartan- (D) treated C57BL/6 mouse. Sections were stained with Hoechst 33342 to identify cell nuclei (blue) and an antibody against CD31 (red) for the detection of microvessels. Scale bars: 50 μm. Immunohistochemical detection of proliferating Ki67-positive cells (arrows) in the stroma of endometriotic lesions of a vehicle-treated control (E) as well as of a parecoxib- (F), a telmisartan- (G) and a parecoxib/telmisartan- (H) treated C57BL/6 mouse. Scale bars: 15 μm. Immunofluorescent detection of apoptotic cells (arrows) within endometriotic lesions of a vehicle-treated control (I) as well as a parecoxib- (J), a telmisartan (K) and a parecoxib/telmisartan- (L) treated C57BL/6 mouse. Sections were stained with Hoechst 33342 to identify cell nuclei (blue) and an antibody against cleaved caspase-3 (casp-3; red) for the detection of apoptotic cells. Scale bars: 20 μm. Microvessel density (M, mm^{-2}), Ki67-positive cells (N, %) and cleaved caspase-3-positive cells (O, %) of endometriotic lesions of vehicle-treated controls (Ctrl), parecoxib- (Pa), telmisartan- (Tel) and parecoxib/telmisartan- (Tel+PA) treated C57BL/6 mice. Means ± SEM ($n = 10$ for each experimental group). $^{*}P < 0.05$ versus control; $^{\#}P < 0.05$ versus parecoxib.

of PPAR-γ, both in the cell nuclei and the cytoplasm (Figure 3G, H).

Furthermore, a significantly lower density of CD31-positive microvessels was detected in telmisartan- and telmisartan/parecoxib-treated lesions when compared with vehicle- and parecoxib-treated lesions (Figure 4A–D, M). Moreover, the number of Ki67-positive proliferating stromal and glandular cells was significantly reduced in lesions exposed to the combination therapy with telmisartan and parecoxib (Figure 4E–H, N).

In addition, endometriotic lesions in vehicle- and parecoxib-treated lesions exhibited no cleaved caspase-3-positive apoptotic cells in the glandular epithelium and only a few apoptotic cells (<1%) in the stroma on day 28 (Figure 4I, J, O). Treatment with telmisartan increased the number of apoptotic stromal cells within the lesions (Figure 4K, O). Of interest, this pro-apoptotic effect of telmisartan was more pronounced in combination with parecoxib treatment (Figure 4L, O).

During the last years, nerve fibre ingrowth into endometriotic lesions has been increasingly suggested to contribute to the generation of chronic pelvic pain in endometriosis patients (Miller and Fraser, 2015). Accordingly, we additionally assessed the density of PGP9.5-positive nerve fibres within the endometriotic lesions on day 28. Of interest, most of these nerve fibres were co-localized with microvessels (Figure 5A). Moreover, we observed a significantly reduced nerve fibre density in telmisartan- and telmisartan/parecoxib-treated lesions when compared with vehicle-treated controls (Figure 5B).

Western blot analysis of endometriotic lesions

Finally, we also analysed the expression levels of selected proteins in the endometriotic lesions on day 28 by means of Western blotting. In line with our previous study (Nenicu *et al.,* 2014), we found that telmisartan treatment significantly increased the expression of COX-2 in the lesions when compared with vehicle-treated controls (Figure 6A, B). In contrast, treatment with parecoxib alone or in combination with telmisartan significantly decreased COX-2 expression (Figure 6A, B). In addition, we detected a markedly higher expression of the apoptosis marker cleaved caspase-3 in telmisartan/parecoxib-treated lesions when compared to the other groups (Figure 6A, C). Accordingly, these lesions also exhibited a reduced expression of the stromal marker vimentin and the angiogenic marker MMP-9 (Figure 6A, D, E). This further indicates the regression of telmisartan/parecoxib-treated endometriotic lesions.

The analysis of intracellular signalling pathways further revealed a significant down-regulation of Akt/eNOS signalling in endometriotic lesions treated with parecoxib, telmisartan or parecoxib/telmisartan when compared with controls (Figure 7A, B, D). In contrast, ERK signalling was significantly up-regulated in telmisartan-treated lesions (Figure 7A, C). However, this telmisartan effect was completely reversed in combination with parecoxib (Figure 7A, C). In addition, expression of cyclin D1, which is a downstream target of both Akt and ERK signalling (Kuo *et al.,* 2017), was significantly down-regulated in the parecoxib/telmisartan-treated lesions when compared with the other groups (Figure 7A, E).

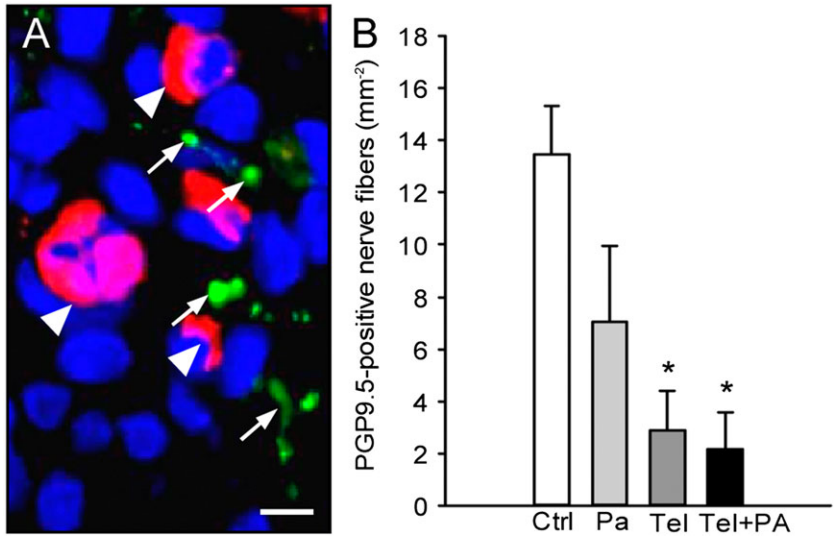

Figure 5

Immunohistochemical analysis of nerve fibre ingrowth into endometriotic lesions. (A) Immunofluorescent detection of microvessels (arrowheads) and nerve fibres (arrows) within an endometriotic lesion on day 28 after surgical induction by fixation of an uterine tissue sample to the abdominal wall of a vehicle-treated control mouse. The section was stained with Hoechst 33342 to identify cell nuclei (blue), an antibody against CD31 (red) for the detection of microvessels and an antibody against PGP9.5 (green) for the detection of nerve fibres. Scale bar: 10 μm. (B) Density of PGP9.5-positive nerve fibres (mm^{-2}) within endometriotic lesions of vehicle-treated controls (Ctrl), parecoxib- (Pa), telmisartan- (Tel) and parecoxib/telmisartan- (Tel+PA) treated C57BL/6 mice. Means ± SEM (n = 10 for each experimental group). *P < 0.05 versus control.

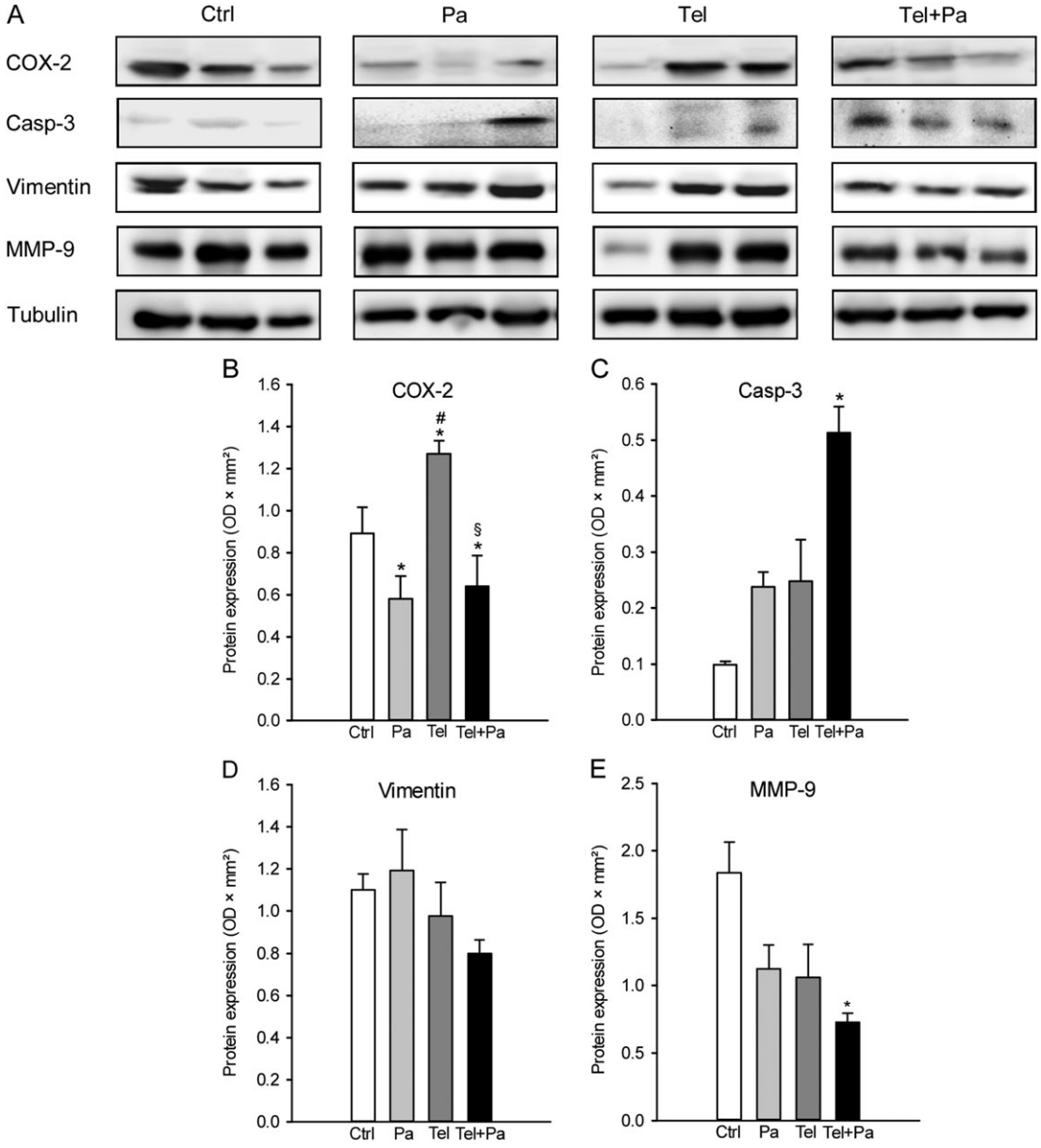

Figure 6

Western blot analysis of endometriotic lesions. (A) Expression of COX-2, cleaved caspase-3 (casp-3), vimentin, MMP-9 and tubulin within endometriotic lesions on day 28 after surgical induction by fixation of uterine tissue samples to the abdominal wall of vehicle-treated control (Ctrl), parecoxib- (Pa), telmisartan- (Tel) and parecoxib/telmisartan-treated (Tel + Pa) C57BL/6 mice as assessed by Western blot analyses. Densitometric analyses of expression (OD × mm^2) of COX-2 (B), cleaved caspase-3 (C), vimentin (D) and MMP-9 (E) within endometriotic lesions of vehicle-treated control (Ctrl), parecoxib- (Pa), telmisartan- (Tel) and parecoxib/telmisartan-(Tel+Pa) treated C57BL/6 mice. Data were normalized to tubulin signals. Means ± SEM ($n = 6$ for each experimental group). *$P < 0.05$ versus control; $^{\#}P < 0.05$ versus parecoxib; $^{\S}P < 0.05$ versus telmisartan.

Discussion

The present study demonstrates that a combination therapy with telmisartan and the COX-2 inhibitor parecoxib is more effective in the treatment of endometriotic lesions than treatment with telmisartan alone. This novel result is in line with the finding that (i) telmisartan and other related antihypertensive drugs, such as losartan, suppress lesion formation in different murine endometriosis models (Nenicu *et al.*, 2014; Cakmak *et al.*, 2015) and that (ii) COX-2 represents a promising target for an analgesic, anti-angiogenic and anti-inflammatory endometriosis therapy (Cobellis *et al.*, 2004; Ozawa *et al.*, 2006; Laschke *et al.*, 2007; Machado *et al.*, 2010; Olivares *et al.*, 2013; Kilico *et al.*, 2014). In fact, telmisartan activates PPAR-γ, which has been shown to enhance COX-2 expression in different cell types (Meade *et al.*, 1999; Ackerman *et al.*, 2005). Hence, the herein observed reverse effect of parecoxib on telmisartan-mediated up-

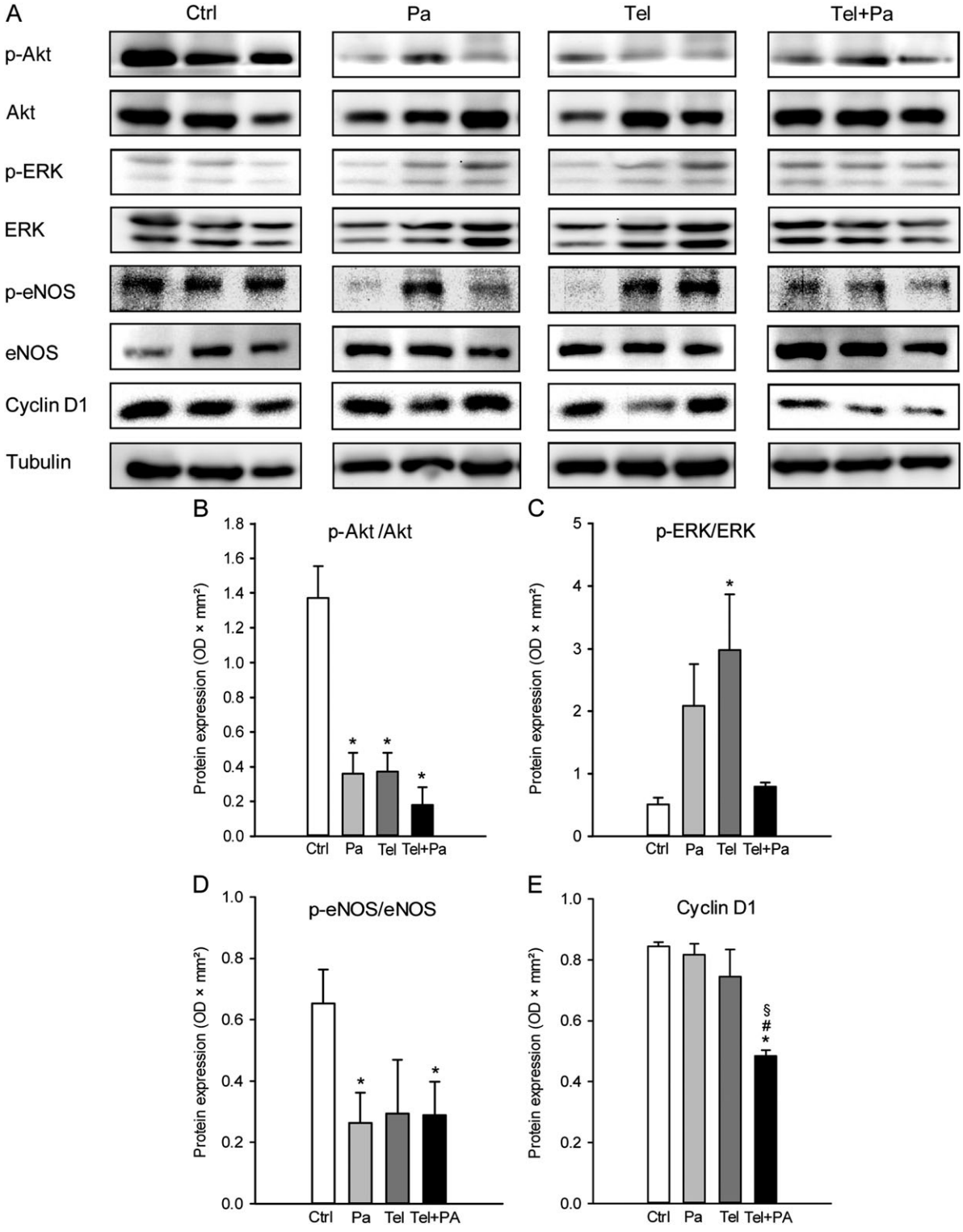

Figure 7

Western blot analysis of endometriotic lesions. (A) Expression of p-Akt, Akt, p-ERK, ERK, p-eNOS, eNOS, cyclin D1 and tubulin within endometriotic lesions on day 28 after surgical induction by fixation of uterine tissue samples to the abdominal wall of vehicle-treated control (Ctrl), parecoxib- (Pa), telmisartan- (Tel) and parecoxib/telmisartan-treated (Tel + Pa) C57BL/6 mice as assessed by Western blot analyses. Densitometric analyses of expression (OD × mm^2) of p-Akt/Akt (B), p-ERK/ERK (C), p-eNOS/eNOS (D) and cyclin D1 (E) within endometriotic lesions of vehicle-treated control (Ctrl), parecoxib- (Pa), telmisartan- (Tel) and parecoxib/telmisartan- (Tel+Pa) treated C57BL/6 mice. Data were normalized to tubulin signals. Means ± SEM (n = 6 for each experimental group). *$P < 0.05$ versus control; $^{\#}P < 0.05$ versus parecoxib; $^{\S}P < 0.05$ versus telmisartan.

regulation of COX-2 expression may have directly potentiated the known beneficial effects of telmisartan treatment on murine endometriotic lesions. Accordingly, our high-resolution ultrasound analyses of the lesions revealed that the treatment with both inhibitors not only suppressed their growth but even resulted in negative lesion and stromal tissue growth rates, indicating a strong regression of the ectopic uterine tissue throughout the 4 week observation period.

Multiple mechanisms may have contributed to the regression of endometriotic lesions. It is well known that the development and survival of endometriotic lesions is crucially dependent on their adequate vascularization (Rocha *et al.,* 2013), which was significantly suppressed in telmisartan-treated animals. This anti-angiogenic effect of the compound is driven by its antagonism of the AT_1 receptor, which inhibits VEGF-induced endothelial cell migration and vascular sprouting (Carbajo-Lozoya *et al.,* 2012). In addition, activation of PPAR-γ has been found to reduce proliferation, migration and tube formation in HUVECs (Sheu *et al.,* 2006) and to suppress vascular network formation in the chorioallantois membrane model (Aljada *et al.,* 2008). In line with these findings, in the present study we observed that the up-regulation of PPAR-γ expression correlated with the reduction of lesion volumes. Thus, telmisartan targets fundamental processes, which are involved in the development of new microvessels. However, we also found that the anti-angiogenic action of telmisartan was not further increased in combination with parecoxib. Moreover, endometriotic lesions treated with parecoxib alone did not exhibit a significantly reduced microvessel density when compared with vehicle-treated controls, although parecoxib and other COX-2 inhibitors have previously been shown to suppress angiogenesis (Laschke *et al.,* 2007; Machado *et al.,* 2010; Olivares *et al.*, 2011). These contradictory findings may be explained by varying experimental settings, including differences in species (rats vs. mice) as well as types, doses and application schemes of the COX-2 inhibitors applied in individual studies.

Suppression of cell proliferation and induction of apoptosis are important mechanisms of action of both COX-2 inhibitors and PPAR-γ agonists (Olivares *et al.,* 2008; Koyama *et al.,* 2014; Pu *et al.,* 2016; Suri *et al.,* 2016). Accordingly, combination therapy with telmisartan and parecoxib markedly reduced the number of Ki67-positive stromal cells and strongly stimulated apoptotic cell death within endometriotic lesions when compared with controls. In line with these results, our Western blot analyses further showed a decreased expression of p-Akt/Akt and downstream p-eNOS/eNOS in parecoxib/telmisartan-treated lesions. Akt signalling is typically up-regulated in endometriosis and promotes the proliferation of endometriotic stromal cells (Cinar *et al.,* 2009; Matsuzaki and Darcha, 2015). Moreover, we detected an increased expression of p-ERK/ERK in telmisartan-treated lesions, confirming reports on the activation of ERK signalling by different PPAR-γ agonists (Chana *et al.,* 2004; Kim *et al.,* 2009). Of interest, we additionally found a significantly down-regulated expression of cyclin D1 in parecoxib/telmisartan-treated lesions when compared to the other groups. Cyclin D1 is an important regulator of cell cycle progression, which is a downstream target of both p-Akt/Akt and p-ERK/ERK signalling (Kuo *et al.,* 2017). Hence, the latter result supports the concept of Matsuzaki and Darcha (2015) that there may be a balanced crosstalk between the Akt and the ERK signalling pathway in endometriosis. They observed an up-regulation of p-ERK/ERK expression in endometriotic stromal cells when p-Akt/Akt expression was decreased and *vice versa*. Similar effects were observed in the present study in parecoxib- and telmisartan-treated lesions. However, the combination of both drugs completely suppressed this interaction. This may be a possible mechanistic explanation for the higher efficacy of the combination therapy when compared with that of telmisartan treatment alone. In fact, parecoxib/telmisartan-treated lesions exhibited a low expression of both p-Akt/Akt and p-ERK/ERK, which was associated with a down-regulated expression of cyclin D1, resulting in a markedly reduced proliferation rate.

Finally, we investigated the ingrowth of PGP9.5-positive nerve fibres into endometriotic lesions, because this process contributes to the pain symptoms of endometriosis patients (Miller and Fraser, 2015). Our immunohistochemical analyses revealed that most nerve fibres were typically co-localized with microvessels. This observation supports the concept of neuroangiogenesis, that is, the close interaction of newly developing microvessels and nerves during physiological development (Weinstein, 2005), which has also been described for the establishment of endometriotic lesions (Asante and Taylor, 2011; Greaves *et al.,* 2014). Of interest, we found a reduced nerve fibre density within telmisartan- and parecoxib/telmisartan-treated endometriotic lesions when compared to vehicle-treated controls. This indicates that these drugs may have also direct beneficial effects on neuroangiogenesis in endometriosis.

In summary, we showed that a pharmacological combination therapy with telmisartan and a COX-2 inhibitor is highly promising for the treatment of endometriosis. Our novel findings not only confirm the results of previous experimental studies, demonstrating that these drugs inhibit the formation of endometriotic lesions (Machado *et al.,* 2010; Nenicu *et al.,* 2014), but also indicate that their combination is even more effective in suppressing cell proliferation and promoting apoptotic cell death within ectopic endometrial tissue. Hence, further studies should now be done to clarify whether these synergistic effects can also be achieved under clinical conditions. This is a realistic goal considering the fact that telmisartan and several COX-2 inhibitors are already approved drugs, which are widely used in patients with tolerable side effect profiles.

Acknowledgements

We are grateful for the technical assistance of Janine Becker and Ruth M. Nickels (Institute for Clinical & Experimental Surgery, Homburg/Saar). This study was partly funded by a grant of the Deutsche Forschungsgemeinschaft (DFG – German Research Foundation) – LA 2682/3-1.

Author contributions

A.N., Y.G. and C.K. performed the research and data acquisition. A.N. and M.W.L. designed the research study, analysed the data and designed the artwork. A.N., M.W.L. and M.D. M. interpreted the data and wrote the paper.

Conflict of interest

The authors declare no conflicts of interest.

Declaration of transparency and scientific rigour

This Declaration acknowledges that this paper adheres to the principles for transparent reporting and scientific rigour of preclinical research recommended by funding agencies, publishers and other organisations engaged with supporting research.

References

Ackerman WE 4th, Zhang XL, Rovin BH, Kniss DA (2005). Modulation of cytokine-induced cyclooxygenase 2 expression by PPARG ligands through NFkappaB signal disruption in human WISH and amnion cells. Biol Reprod 73: 527–535.

Alexander SPH, Davenport AP, Kelly E, Marrion N, Peters JA, Benson HE *et al.* (2015a). The Concise Guide to PHARMACOLOGY 2015/16: G protein-coupled receptors. Br J Pharmacol 172: 5744–5869.

Alexander SPH, Cidlowski JA, Kelly E, Marrion N, Peters JA, Benson HE *et al.* (2015b). The Concise Guide to PHARMACOLOGY 2015/16: Nuclear hormone receptors. Br J Pharmacol 172: 5956–5978.

Alexander SPH, Fabbro D, Kelly E, Marrion N, Peters JA, Benson HE *et al.* (2015c). The Concise Guide to PHARMACOLOGY 2015/16: Enzymes. Br J Pharmacol 172: 6024–6109.

Aljada A, O'Connor L, Fu YY, Mousa SA (2008). PPAR gamma ligands, rosiglitazone and pioglitazone, inhibit bFGF- and VEGF-mediated angiogenesis. Angiogenesis 11: 361–367.

Asante A, Taylor RN (2011). Endometriosis: the role of neuroangiogenesis. Annu Rev Physiol 73: 163–182.

Banu SK, Lee J, Speights VO Jr, Starzinski-Powitz A, Arosh JA (2008). Cyclooxygenase-2 regulates survival, migration, and invasion of human endometriotic cells through multiple mechanisms. Endocrinology 149: 1180–1189.

Becker CM, Wright RD, Satchi-Fainaro R, Funakoshi T, Folkman J, Kung AL *et al.* (2006). A novel noninvasive model of endometriosis for monitoring the efficacy of antiangiogenic therapy. Am J Pathol 168: 2074–2084.

Buchweitz O, Staebler A, Wülfing P, Hauzman E, Greb R, Kiesel L (2006). COX-2 overexpression in peritoneal lesions is correlated with nonmenstrual chronic pelvic pain. Eur J Obstet Gynecol Reprod Biol 124: 216–221.

Burney RO, Giudice LC (2012). Pathogenesis and pathophysiology of endometriosis. Fertil Steril 98: 511–519.

Cakmak B, Cavusoglu T, Ates U, Meral A, Nacar MC, Erbaş O (2015). Regression of experimental endometriotic implants in a rat model with the angiotensin II receptor blocker losartan. J Obstet Gynaecol Res 41: 601–607.

Carbajo-Lozoya J, Lutz S, Feng Y, Kroll J, Hammes HP, Wieland T (2012). Angiotensin II modulates VEGF-driven angiogenesis by opposing effects of type 1 and type 2 receptor stimulation in the microvascular endothelium. Cell Signal 24: 1261–1269.

Chana RS, Lewington AJ, Brunskill NJ (2004). Differential effects of peroxisome proliferator activated receptor-gamma (PPAR gamma) ligands in proximal tubular cells: thiazolidinediones are partial PPAR gamma agonists. Kidney Int 65: 2081–2090.

Cinar O, Seval Y, Uz YH, Cakmak H, Ulukus M, Kayisli UA *et al.* (2009). Differential regulation of Akt phosphorylation in endometriosis. Reprod Biomed Online 19: 864–871.

Cobellis L, Razzi S, De Simone S, Sartini A, Fava A, Danero S *et al.* (2004). The treatment with a COX-2 specific inhibitor is effective in the management of pain related to endometriosis. Eur J Obstet Gynecol Reprod Biol 116: 100–102.

Curtis MJ, Bond RA, Spina D, Ahluwalia A, Alexander SP, Giembycz MA *et al.* (2015). Experimental design and analysis and their reporting: new guidance for publication in BJP. Br J Pharmacol 172: 3461–3471.

Giudice LC (2010). Clinical practice. Endometriosis. N Engl J Med 362: 2389–2398.

Greaves E, Collins F, Esnal-Zufiaurre A, Giakoumelou S, Horne AW, Saunders PT (2014). Estrogen receptor (ER) agonists differentially regulate neuroangiogenesis in peritoneal en-dometriosis via the repellent factor SLIT3. Endocrinology 155: 4015–4026.

Grümmer R (2006). Animal models in endometriosis research. Hum Reprod Update 12: 641–649.

Jiang L, Yan Y, Liu Z, Wang Y (2016). Inflammation and endometriosis. Front Biosci (Landmark Ed) 21: 941–948.

Kilico I, Kokcu A, Kefeli M, Kandemir B (2014). Regression of experimentally induced endometriosis with a new selective cyclooxygenase-2 enzyme inhibitor. Gynecol Obstet Invest 77: 35–39.

Kilkenny C, Browne W, Cuthill IC, Emerson M, Altman DG (2010). Animal research: reporting in vivo experiments: the ARRIVE guidelines. Br J Pharmacol 160: 1577–1579.

Kim J, Han DC, Kim JM, Lee SY, Kim SJ, Woo JR *et al.* (2009). PPAR gamma partial agonist, KR-62776, inhibits adipocyte differentiation via activation of ERK. Cell Mol Life Sci 66: 1766–1781.

Körbel C, Menger MD, Laschke MW (2010). Size and spatial orientation of uterine tissue transplants on the peritoneum crucially determine the growth and cyst formation of endometriosis-like lesions in mice. Hum Reprod 25: 2551–2558.

Koyama N, Nishida Y, Ishii T, Yoshida T, Furukawa Y, Narahara H (2014). Telmisartan induces growth inhibition, DNA double-strand breaks and apoptosis in human endometrial cancer cells. PLoS One 9: e93050.

Kuo YH, Chiang EI, Chao CY, Rodriguez RL, Chou PY, Tsai SY *et al.* (2017). Dual inhibition of key proliferation signaling pathways in triple-negative breast cancer cells by a novel derivative of Taiwanin A. Mol Cancer Ther 16: 480–493.

Laschke MW, Elitzsch A, Scheuer C, Vollmar B, Menger MD (2007). Selective cyclo-oxygenase-2 inhibition induces regression of autologous endometrial grafts by down-regulation of vascular endothelial growth factor-mediated angiogenesis and stimulation of caspase-3-dependent apoptosis. Fertil Steril 87: 163–171.

Laschke MW, Giebels C, Menger MD (2011). Vasculogenesis: a new piece of the endometriosis puzzle. Hum Reprod Update 17: 628–636.

Laschke MW, Körbel C, Rudzitis-Auth J, Gashaw I, Reinhardt M, Hauff P *et al.* (2010). High-resolution ultrasound imaging: a novel technique for the noninvasive in vivo analysis of endometriotic

lesion and cyst formation in small animal models. Am J Pathol 176: 585–593.

Laschke MW, Menger MD (2012). Anti-angiogenic treatment strategies for the therapy of endometriosis. Hum Reprod Update 18: 682–702.

Machado DE, Berardo PT, Landgraf RG, Fernandes PD, Palmero C, Alves LM *et al.* (2010). A selective cyclooxygenase-2 inhibitor suppresses the growth of endometriosis with an antiangiogenic effect in a rat model. Fertil Steril 93: 2674–2679.

Matsuzaki S, Darcha C (2015). Co-operation between the AKT and ERK signaling pathways may support growth of deep endometriosis in a fibrotic microenvironment in vitro. Hum Reprod 30: 1606–1616.

McGrath JC, Lilley E (2015). Implementing guidelines on reporting research using animals (ARRIVE etc.): new requirements for publication in BJP. Br J Pharmacol 172: 3189–3193.

Meade EA, McIntyre TM, Zimmerman GA, Prescott SM (1999). Peroxisome proliferators enhance cyclooxygenase-2 expression in epithelial cells. J Biol Chem 274: 8328–8334.

Miller EJ, Fraser IS (2015). The importance of pelvic nerve fibers in endometriosis. Womens Health (Lond) 11: 611–618.

Nenicu A, Körbel C, Gu Y, Menger MD, Laschke MW (2014). Combined blockade of angiotensin II type 1 receptor and activation of peroxisome proliferator-activated receptor-γ by telmisartan effectively inhibits vascularization and growth of murine endometriosis-like lesions. Hum Reprod 29: 1011–1024.

Olivares C, Bilotas M, Buquet R, Borghi M, Sueldo C, Tesone M *et al.* (2008). Effects of a selective cyclooxygenase-2 inhibitor on endometrial epithelial cells from patients with endometriosis. Hum Reprod 23: 2701–2708.

Olivares C, Ricci A, Bilotas M, Barañao RI, Meresman G (2011). The inhibitory effect of celecoxib and rosiglitazone on experimental endometriosis. Fertil Steril 96: 428–433.

Olivares CN, Bilotas MA, Ricci AG, Barañao RI, Meresman GF (2013). Anastrozole and celecoxib for endometriosis treatment, good to keep them apart? Reproduction 145: 119–126.

Ozawa Y, Murakami T, Tamura M, Terada Y, Yaegashi N, Okamura K (2006). A selective cyclooxygenase-2 inhibitor suppresses the growth of endometriosis xenografts via antiangiogenic activity in severe combined immunodeficiency mice. Fertil Steril 86: 1146–1151.

Pu Z, Zhu M, Kong F (2016). Telmisartan prevents proliferation and promotes apoptosis of human ovarian cancer cells through upregulating PPARγ and downregulating MMP-9 expression. Mol Med Rep 13: 555–559.

Rocha AL, Reis FM, Taylor RN (2013). Angiogenesis and endometriosis. Obstet Gynecol Int 2013: 859619.

Rudzitis-Auth J, Körbel C, Scheuer C, Menger MD, Laschke MW (2012). Xanthohumol inhibits growth and vascularization of developing endometriotic lesions. Hum Reprod 27: 1735–1744.

Rudzitis-Auth J, Menger MD, Laschke MW (2013). Resveratrol is a potent inhibitor of vascularization and cell proliferation in experimental endometriosis. Hum Reprod 28: 1339–1347.

Sheu WH, Ou HC, Chou FP, Lin TM, Yang CH (2006). Rosiglitazone inhibits endothelial proliferation and angiogenesis. Life Sci 78: 1520–1528.

Simoens S, Dunselman G, Dirksen C, Hummelshoj L, Bokor A, Brandes I *et al.* (2012). The burden of endometriosis: costs and quality of life of women with endometriosis and treated in referral centres. Hum Reprod 27: 1292–1299.

Somigliana E, Vigano P, Benaglia L, Busnelli A, Vercellini P, Fedele L (2012). Adhesion prevention in endometriosis: a neglected critical challenge. J Minim Invasive Gynecol 19: 415–421.

Southan C, Sharman JL, Benson HE, Faccenda E, Pawson AJ, Alexander SP *et al.* (2016). The IUPHAR/BPS Guide to PHARMACOLOGY in 2016: towards curated quantitative interactions between 1300 protein targets and 6000 ligands. Nucleic Acids Res 44: D1054–D1068.

Suri A, Sheng X, Schuler KM, Zhong Y, Han X, Jones HM *et al.* (2016). The effect of celecoxib on tumor growth in ovarian cancer cells and a genetically engineered mouse model of serous ovarian cancer. Oncotarget 7: 39582–39594.

Weinstein BM (2005). Vessels and nerves: marching to the same tune. Cell 120: 299–302.

Wu MH, Lu CW, Chuang PC, Tsai SJ (2010). Prostaglandin E2: the master of endometriosis? Exp Biol Med (Maywood) 235: 668–677.